





# SCIENTIFIC REPORTS



OPEN

## Molecular subtypes of Alzheimer's disease

Giuseppe Di Fede<sup>1</sup>, Marcella Catania<sup>1</sup>, Emanuela Maderna<sup>1</sup> , Roberta Ghidoni<sup>2</sup>, Luisa Benussi<sup>2</sup> , Elisa Tonoli<sup>2</sup>, Giorgio Giaccone<sup>1</sup>, Fabio Moda<sup>1</sup>, Anna Paterlini<sup>2</sup>, Ilaria Campagnani<sup>1</sup>, Stefano Sorrentino<sup>1</sup> , Laura Colombo<sup>3</sup>, Adriana Kubis<sup>1,4</sup>, Edoardo Bistaffa<sup>1</sup>, Bernardino Ghetti<sup>1</sup>  & Fabrizio Tagliavini<sup>1</sup>

Received: 24 October 2017

Accepted: 7 February 2018

Published online: 19 February 2018

Protein misfolding and aggregation is a central feature of several neurodegenerative disorders including Alzheimer's disease (AD), in which assemblies of amyloid  $\beta$  ( $A\beta$ ) peptides accumulate in the brain in the form of parenchymal and/or vascular amyloid. A widely accepted concept is that AD is characterized by distinct clinical and neuropathological phenotypes. Recent studies revealed that  $A\beta$  assemblies might have structural differences among AD brains and that such pleomorphic assemblies can correlate with distinct disease phenotypes. We found that in both sporadic and inherited forms of AD, amyloid aggregates differ in the biochemical composition of  $A\beta$  species. These differences affect the physicochemical properties of  $A\beta$  assemblies including aggregation kinetics, resistance to degradation by proteases and seeding ability.  $A\beta$ -amyloidosis can be induced and propagated in animal models by inoculation of brain extracts containing aggregated  $A\beta$ . We found that brain homogenates from AD patients with different molecular profiles of  $A\beta$  are able to induce distinct patterns of  $A\beta$ -amyloidosis when injected into mice. Overall these data suggest that the assembly of mixtures of  $A\beta$  peptides into different  $A\beta$  seeds leads to the formation of distinct subtypes of amyloid having distinctive physicochemical and biological properties which result in the generation of distinct AD molecular subgroups.

Misfolding, aggregation and deposition of amyloid  $\beta$  ( $A\beta$ ) peptides in brain parenchyma and vessel walls are regarded as key events in the pathogenic cascade of Alzheimer's disease (AD)<sup>1,2</sup>.  $A\beta$  fragments of various lengths are generated by cleavage of the amyloid precursor protein (APP) by  $\beta$ - and  $\gamma$ -secretases, and subsequent digestion by endogenous proteases. This process results in the formation of a variety of N- and C-terminal-truncated  $A\beta$  species<sup>1,3-5</sup> having the ability to assemble into abnormal aggregates<sup>6-8</sup>.

During the past few years, a great number of studies have pointed to the  $A\beta$  aggregates as key determinants in the molecular machinery leading to AD<sup>9,10</sup>. Moreover, it has been suggested that different  $A\beta$  assemblies exist, each defined by distinct molecular size, stability and neurotoxic properties<sup>11</sup>. However, their specific relevance in AD pathogenesis is unclear. In addition, the existence of different N-terminal and C-terminal truncated forms of  $A\beta$  in AD brain is now well known<sup>12,13</sup>. As for  $A\beta$  aggregates, we actually don't know if different  $A\beta$  monomeric isoforms play a role in determining specific molecular AD phenotypes.

AD comprises different phenotypes characterized by diverse clinical presentations, neuroanatomical involvement and neuropathological profiles. Although this phenotypic heterogeneity is most striking in the dominantly inherited forms, it is also well recognized in sporadic cases. The molecular basis of these phenotypic variations is largely unknown<sup>14-16</sup>.

Previous studies showed that  $A\beta$  deposits differ in morphology and biochemical composition among individuals with AD, and among APP transgenic mouse models<sup>17-22</sup>. The existence of different  $A\beta$  "morphotypes" is further supported by the finding of distinct structural variants of  $A\beta$  fibrils isolated from brain of AD patients<sup>23,24</sup>.

It has been hypothesized that spread of  $A\beta$  aggregates from region to region may account for propagation of the disease process and neurodegeneration, with mechanisms analogous to spreading of the pathogenic forms of

<sup>1</sup>IRCCS Foundation "Carlo Besta" Neurological Institute, Milan, Italy. <sup>2</sup>Molecular Markers Laboratory, IRCCS Istituto Centro San Giovanni di Dio - Fatebenefratelli, Brescia, Italy. <sup>3</sup>Department of Molecular Biochemistry and Pharmacology, IRCCS Istituto di Ricerche Farmacologiche "Mario Negri", Milan, Italy. <sup>4</sup>Department of Toxicology, Wroclaw Medical University, Wroclaw, Poland. <sup>5</sup>Department of Pathology and Laboratory Medicine, Indiana University, Indianapolis, Indiana, USA. Correspondence and requests for materials should be addressed to F.T. (email: [fabrizio.tagliavini@istituto-besta.it](mailto:fabrizio.tagliavini@istituto-besta.it))

the prion protein (PrP<sup>Res</sup>) in transmissible spongiform encephalopathies<sup>25</sup>. This hypothesis is based on experimental evidence that A $\beta$  amyloidosis can be induced in animal models by inoculation of brain extracts containing aggregated A $\beta$ <sup>26,27</sup>, and distinct types of A $\beta$  aggregates can reproduce the neuropathological profile of the donor in a given transgenic mouse line<sup>28</sup>.

The aims of this study were: (i) to investigate whether a molecular heterogeneity based on the existence of distinct profiles of A $\beta$  aggregates occurs in AD; (ii) to define the molecular features characterizing distinct A $\beta$  assemblies and test the hypothesis that differences in molecular profiles affect the physicochemical properties of A $\beta$  assemblies, which can be involved in the generation of different AD phenotypes.

We found that in both sporadic and genetically determined forms of AD, amyloid aggregates show differences in the biochemical composition of A $\beta$  species. Such differences are associated with changes in aggregation kinetics, resistance to protease degradation, seeding activity *in vitro*, and ability to induce amyloidosis in animal models.

These findings support the hypothesis that the variability of AD phenotypes may result from a potential multiplicity of A $\beta$  aggregation modalities. Accordingly, a detailed analysis of A $\beta$  aggregation and seeding properties may lead to a novel classification of AD, based on the identification of subtypes of A $\beta$ 's distinct macromolecular aggregates.

## Results

### AD patients are highly heterogeneous regarding the morphologic characteristics of A $\beta$ deposits.

A neuropathological study in a cohort consisting of 20 patients with sporadic AD (indicated as sAD1–sAD20 numbered in Table S1), and 4 patients with familial AD associated with APP, PS1 or PS2 mutations - fAD-APP<sub>A673V</sub>, fAD-APP<sub>A713T</sub>, fAD-PS1<sub>P117A</sub> and fAD-PS2<sub>A85V</sub> - (indicated as fAD1–4 in Table S1), showed the common typical changes of AD consisting of parenchymal (*amyloid plaques*) and vascular (*congophilic amyloid angiopathy*, CAA) amyloid deposits, neurofibrillary tangles, neuropil threads and dystrophic neurites containing hyperphosphorylated tau, accompanied by neuronal loss, astrogliosis and microglial activation throughout the cerebral cortex. However, an in-depth examination of the amyloid- $\beta$  pathology revealed the existence of dissimilarities concerning density, shape and size as well as the relative severity of parenchymal versus vascular deposition of amyloid in the brain (Fig. 1). In particular, the A673V mutation (fAD1) (a,f,k panels), whose full neuropathological assessment was previously described<sup>29</sup>, showed abundant amyloid deposits both in the parenchyma and in the vessels, immunoreactive for antibodies recognizing epitopes spanning overall the A $\beta$  sequence. Many small vessels in parenchyma and leptomeninges showed thickening of the walls due to the accumulation of amyloid and 'drusige Entartung'. Pathological hallmarks of APP<sub>A713T</sub> (fAD2) (b,g,l panels) were CAA and low-density parenchymal A $\beta$  amyloid deposits in the neuropil. Severe amyloid deposition affected leptomeningeal and small parenchymal vessels in the cerebral hemisphere. Affected vessels were disrupted with amyloid assuming a radial appearance, thickening and double barreling of the wall, loss of smooth muscle cells and narrowing of the lumina. Neuropathological analysis of the PS1<sub>P117A</sub> case (fAD3) (c,h,m panels) was remarkable for numerous and widespread plaques in all cortical layers with higher density in the subpial region. The two sporadic cases showed completely different amyloid patterns, one (sAD1) (d,i,n panels) with predominance of vascular amyloid deposits and capillary A $\beta$  deposition spreading from the vessel walls into the surrounding neuropil ('drusige Entartung'), and mature plaques sparse in cerebral cortex, the other (sAD6) (e,j,o panels) characterized by tiny and diffuse plaques distributed over all cortical layers, with focal and mild CAA.

This observation suggested that, just considering the morphology and distribution of A $\beta$  deposits, the neuropathology of AD is extremely variable not only among genetic cases but also among sporadic patients.

**AD patients have distinct amyloid- $\beta$  profiles.** Following the hypothesis that changes in A $\beta$  pathology may be due to differences in the molecular composition of amyloid, we extracted and purified parenchymal amyloid from the brains of the sAD1–20 and the fAD1–4 patients and analyzed its A $\beta$  content by an immunoproteomic assay. The study revealed that different A $\beta$  isoforms, including N- and C-terminally truncated species, contribute to amyloid composition and that the relative amounts of such peptides can vary among AD brains.

These data led to the identification of two main AD subgroups, each characterized by distinctive profiles of A $\beta$  species (Table 1 and Fig. 2), indicated as Amyloid Profile 1 (AP1) and Amyloid Profile 2 (AP2). AP1 was found in 14 sAD patients and in the individuals with presenilin mutations, while AP2 was detected in five sAD cases. AP1 was marked by a high relative proportion of A $\beta$ X-42 peptides, especially A $\beta$ 1-42, A $\beta$ 4-42, A $\beta$ 11-42 and the pyroglutamate-modified A $\beta$ 3pE-42 and A $\beta$ 11pE-42, while AP2 was distinguished by the presence of both A $\beta$ X-40 and A $\beta$ X-42 peptides, with a prevalence of the former, and minor species including N- and C-terminal truncated forms, such as A $\beta$ 2-39. The two patients with the APP mutations showed a distinct amyloid profile, designated as AP3, mainly composed by A $\beta$ 1-40, A $\beta$ 1-38 and A $\beta$ 1-37. Finally, one individual with sAD (sAD1), neuropathologically characterized by very severe CAA (panels d,i,n in Fig. 1) exhibited a peculiar profile with a predominance of A $\beta$ 1-40, A $\beta$ 3pE-40 and A $\beta$ 1-36 isoforms.

According to these data, Table 1 shows a molecular stratification of our series of AD cases into three distinct subgroups (AP1–AP3). sAD1, whose molecular profile cannot be included in the other groups, is also reported.

As detailed in the "Supplementary Information" online section, neuropathological studies provided evidence of heterogeneity of patterns of A $\beta$  deposition among both familial and sporadic AD patients (Table S1). However, when we searched for correlations between the molecular and the neuropathological profiles within the same AD subgroup, we did not find a clear-cut link between the two variables. These data suggest that the pathologic changes occurring in AD brains are the result of a combination of molecular mechanisms involving not only A $\beta$  peptides but also additional molecules, such as tau and other unexplored or thoroughly unknown factors.



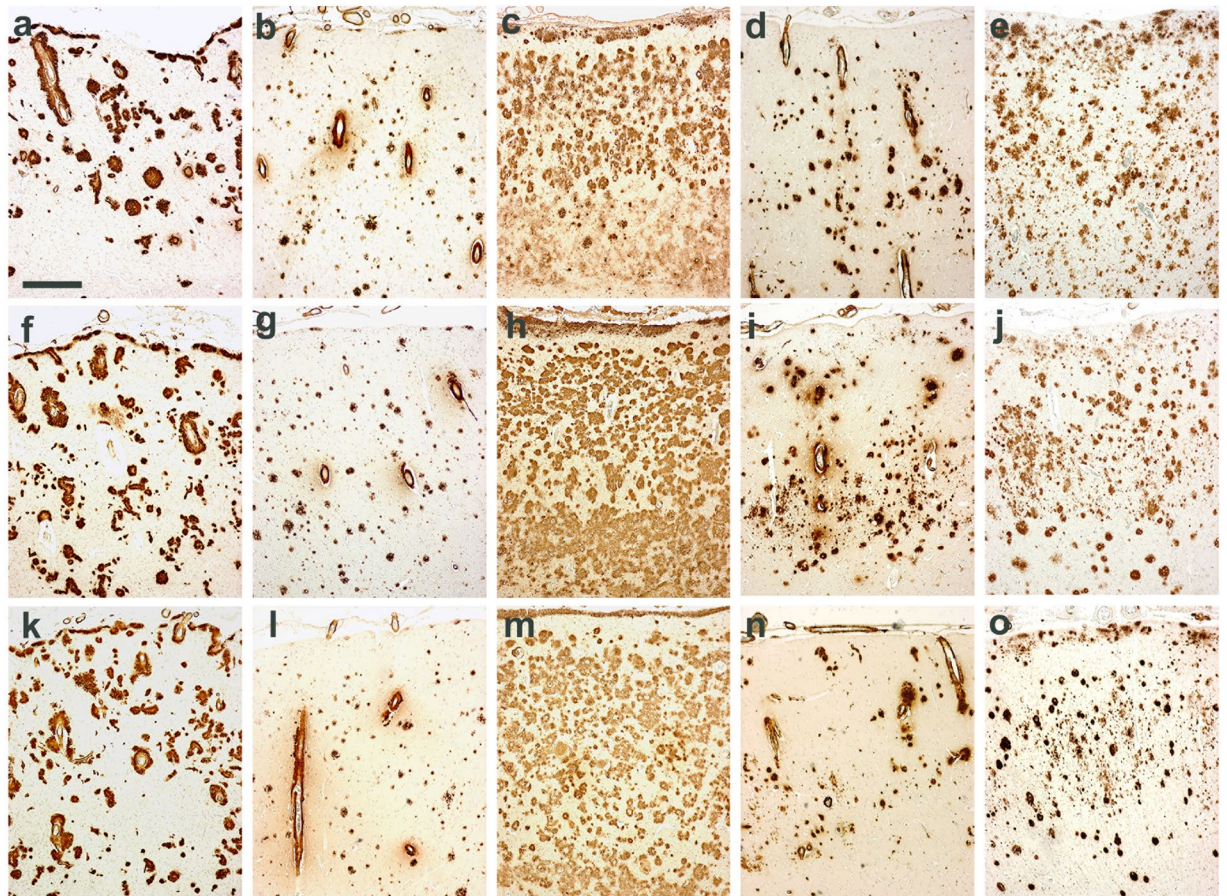


**Figure 1.** Differences in amyloid-related pathology of AD cases. (a,f,k)  $APP_{A673V}$  (fAD1 in Table S1); (b,g,l)  $APP_{A713V}$  (fAD2 in Table S1); (c,h,m)  $PS1_{P117A}$  (fAD3 in Table S1); (d,i,n) sAD carrying the ApoE  $\epsilon 4/\epsilon 4$  genotype (sAD1 in Table S1); (e,j,o) sAD  $\epsilon 3/\epsilon 3$  (sAD6 in Table S1). Scale bar = 400  $\mu m$ . (a,b,c,d,e) frontal cortex; (f,g,h,i,j) temporal cortex; (k,l,m,n,o) occipital cortex. Immunohistochemical study performed using the 4G8 antibody against A $\beta$ .

Profile	Case	Main A $\beta$ peptides	Apo E genotype
AP1	fAD3 ( $PS1_{P117A}$ ), fAD4 ( $PS2_{A85V}$ ), sAD2, sAD3, sAD4, sAD5, sAD6, sAD7, sAD8, sAD10, sAD12, sAD14, sAD15, sAD18, sAD19, sAD20	A $\beta$ 1-42, A $\beta$ 4-42, A $\beta$ 3pE-42, A $\beta$ 11pE-42	$\epsilon 2 = 9.4\%$ $\epsilon 3 = 68.7\%$ $\epsilon 4 = 21.9\%$ $\epsilon 2 = 10.0\%$
AP2	sAD9, sAD11, sAD13, sAD16, sAD17	A $\beta$ 1-40, A $\beta$ 1-42	$\epsilon 3 = 30.0\%$ $\epsilon 4 = 60.0\%$
AP3	fAD1 ( $APP_{A673V}$ ), fAD2 ( $APP_{A713T}$ )	A $\beta$ 1-40, A $\beta$ 1-38, A $\beta$ 1-37	$\epsilon 3 = 100\%$
—	sAD1	A $\beta$ 1-40, A $\beta$ 3pE-40, A $\beta$ 1-36	$\epsilon 4 = 100\%$

**Table 1.** Molecular grouping of Alzheimer's disease cases based on A $\beta$  content in amyloid.

**Distinct molecular profiles of AD show differences in their aggregation pathways.** We then investigated whether the soluble fraction of brain homogenates from patients with different A $\beta$  profiles has different ability to aggregate *in vitro* using ThT assays. The analysis showed that *de novo* amyloidogenesis differed among the two main molecular subgroups of AD, in that the AP1 aggregation kinetics was faster than AP2 samples. The samples from APP-mutated patients (AP3) showed an aggregation pattern slower than the other subgroups during the time-course of the study. On the opposite, aggregation kinetics was especially rapid for sAD1 brain sample (Fig. 3a,b).

Brain extracts immunodepleted from A $\beta$  did not show any aggregation, indicating that A $\beta$  peptides are the aggregating species in the setting of this assays (data not shown).

**Distinct molecular subgroups of AD have different seeding abilities.** RT-QuIC was used to assess the seeding effects of the molecular subgroups of AD on synthetic wild-type A $\beta$ 1-42 (A $\beta$ 1-42<sub>WT</sub>) substrate (Fig. 4a). The study revealed that brain extracts from individuals belonging to AP1 and AP2, and the sAD1 case

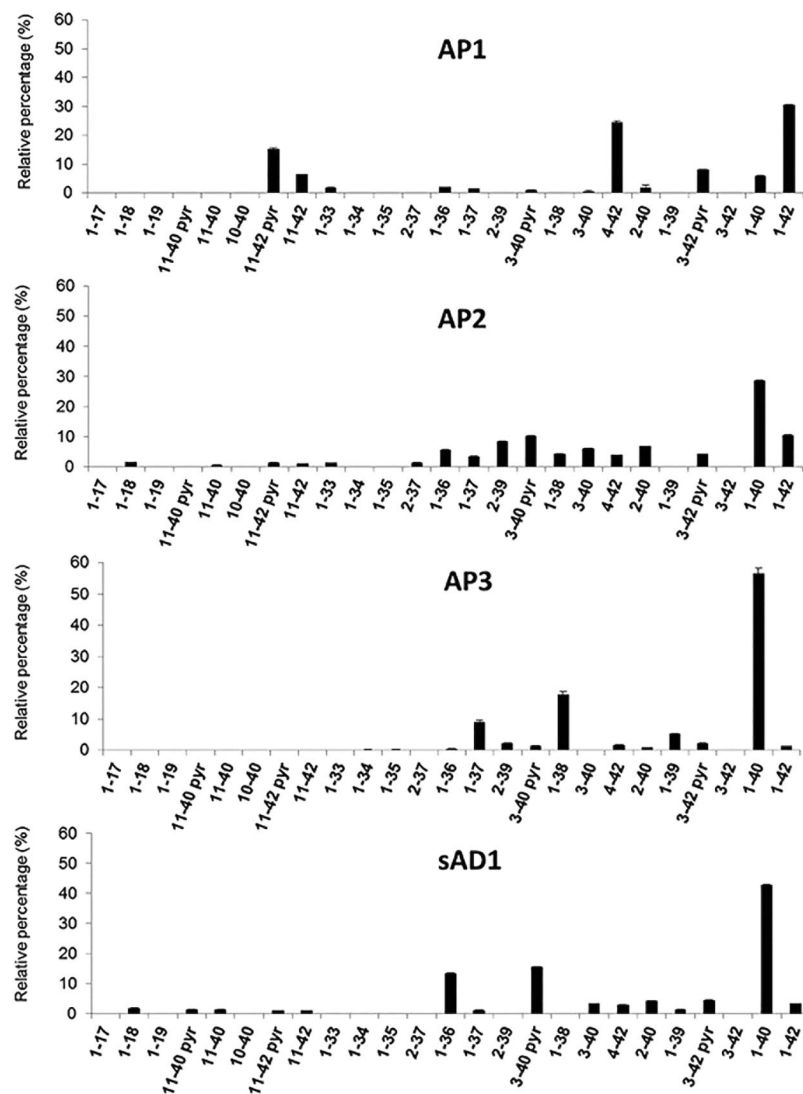


**Figure 2.** A $\beta$  isoforms' fingerprints. A $\beta$  isoforms were analyzed by immunoproteomic analysis, performed using two different A $\beta$  monoclonal antibodies (6E10 and 4G8) on pre-activated chip array, followed by mass spectrometry. Relative percentage of A $\beta$  peptides (with respect to the total A $\beta$  amount) as measured in human brains; for each AD subgroup a representative profile is reported (n = 3, mean relative percentages  $\pm$  SEM (AP1 to AP3 numbering; sAD1 profile is reported outside of the other groups for its peculiarities).

had seeding activities, since they shorten the lag phase of aggregation kinetics of synthetic A $\beta$ 1-42<sub>WT</sub> (Fig. 4a). The results were mostly consistent with those observed in the previous experiment in that (i) AP1 showed a seeding activity higher than AP2 and (ii) the sAD1 sample induced the fastest aggregation of A $\beta$ 1-42 which, under this experimental setting, showed a steeper slope in the polymerization step of kinetics. In contrast, brain extracts from APP-mutated patients (AP3) showed a weak ability of inducing the aggregation of the A $\beta$ 1-42<sub>WT</sub> substrate and followed different aggregation kinetics. Interestingly, the aggregation kinetics induced by the brain extract from the APP<sub>A673V</sub> homozygous patient are faster when we used the mutated A $\beta$  peptide (i.e., A $\beta$ 1-42 carrying the A673V mutation) as substrate in the RT-QuIC assay, suggesting that the affinity between seed and monomer is one of the modifiers of the aggregation profile (Fig. 4b).

APP<sub>A713T</sub> shows high ThT signal at the beginning of the assay. This may be due to a very fast recruitment of the substrate that leads to the early saturation of ThT. The decrease of the signal in the rest of the curve may be caused by the instability of the aggregates generated by this brain extract along the course of the assay.

RT-QuIC performed on A $\beta$ 1-42<sub>WT</sub> peptide co-incubated with brain extracts from control group (i.e., nondemented subjects without neuropathological changes) and from immunodepleted controls (Fig. S1) did not show any aggregation during the time course of the experiments.

RT-QuIC assay was also carried out using a synthetic wild-type A $\beta$ 1-40 substrate (Fig. S2). In this case, no substantial differences were observed among the brain extracts of the different subgroups, suggesting that A $\beta$ 1-40 is not a useful substrate to detect variances in seeding abilities of distinct AD subgroups.

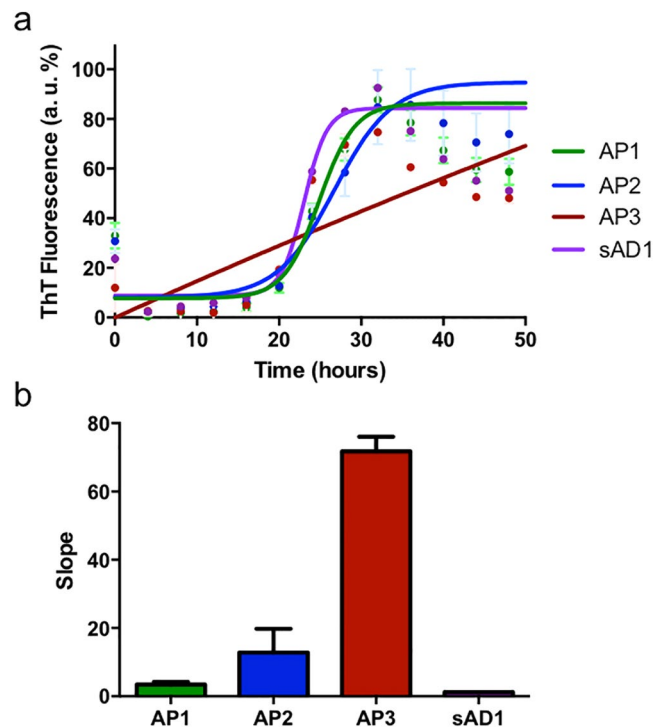


**Figure 3.** Aggregation pathways of different A $\beta$  seeds by ThT assays. Aggregation kinetics of distinct AD A $\beta$  profiles (AP1-AP3 and sAD1 case) were analyzed by ThT assays. Soluble fractions from AD brain homogenates were diluted in 100 mM Tris-HCl pH 7.5, 5  $\mu$ M ThT. ThT intensity was normalized to the corresponding maximal ThT fluorescence and fitted using Boltzmann equation (a). The kinetics were compared by considering the slope of the normalized curves described by ThT fluorescence emission (b).

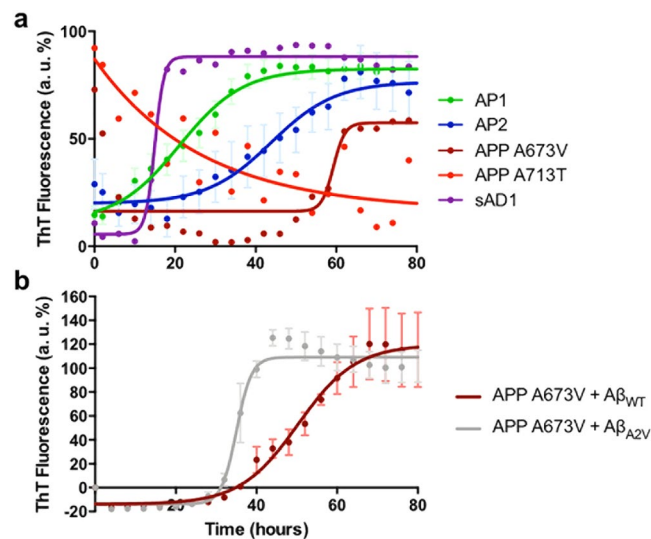


**Figure 4.** RT-QuIC profiles of human brain extracts from the molecular subgroups of AD. Soluble fractions from AD brain homogenates were diluted in 100 mM Tris-HCl pH 7.5, 5  $\mu$ M ThT, 4  $\mu$ M A $\beta$ <sub>1-42</sub><sub>WT</sub> (panel a) or A $\beta$ <sub>1-42</sub><sub>A2V</sub> (panel b). ThT intensity was normalized to the corresponding maximal ThT fluorescence and expressed as relative arbitrary units (a. u. %). Comparison of aggregation kinetics of brain extracts from AP1 and AP2 profiles and APP<sub>A673V</sub>, APP<sub>A713T</sub> and sAD1 subjects (a). Each brain sample was analyzed in quadruplicate. Data are shown as mean  $\pm$  SEM. Comparison of aggregation kinetics of APP<sub>A673V</sub> brain extract when co-incubated with A $\beta$ <sub>1-42</sub> wild-type or A $\beta$ <sub>1-42</sub> carrying the A2V mutation, corresponding to A673V substitution on APP gene (b). Each brain sample was analyzed in triplicate. Data are shown as mean  $\pm$  SEM.



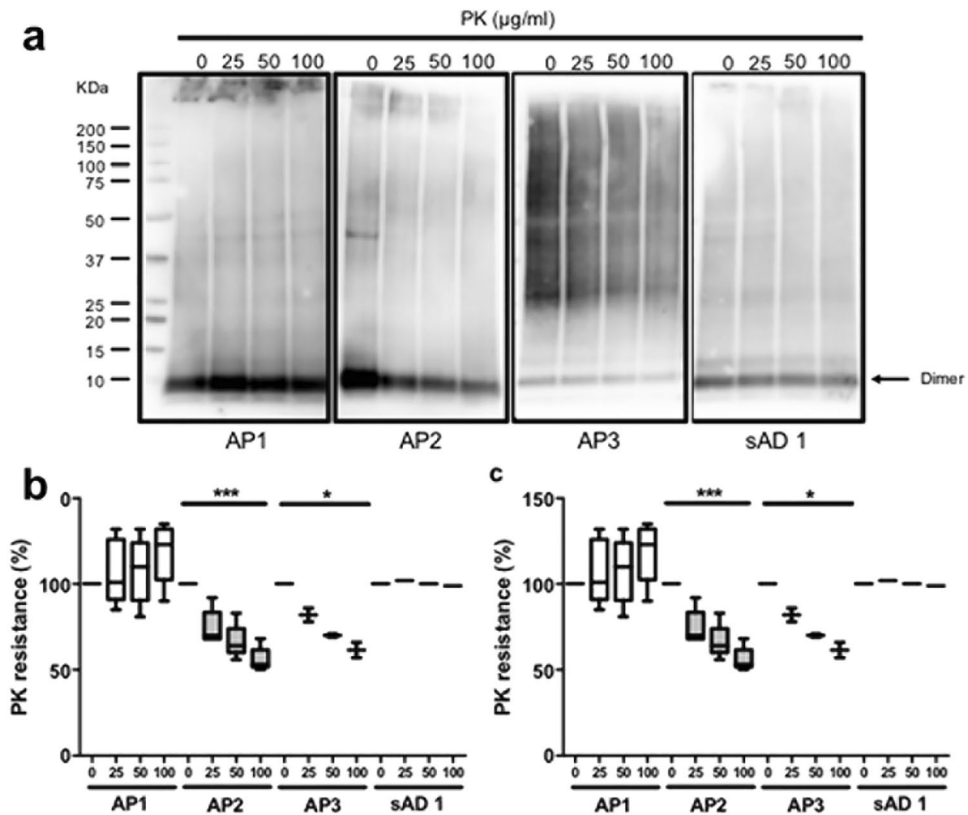


**Figure 5.** PK resistance of A $\beta$ -containing human brain extracts. Insoluble fractions from AD brain homogenates were digested with 0, 25, 50, 100  $\mu$ g/ml of PK and analyzed by Western blot using 4G8 antibody. The signal intensity of all the A $\beta$  aggregates (a,b) or of A $\beta$  dimers (a,c) was quantified by densitometry; data were compared by two-ways ANOVA (\* $p < 0.05$ ; \*\*\* $p < 0.001$ ). Each blot shows the digestion of one brain extract representative of each amyloid profile. The blots were cropped; the original blots are shown in Supplementary Figure S3.

**A $\beta$  aggregates from AD molecular subgroups show different resistance to degradation.** The resistance of A $\beta$  aggregates to proteolysis was assessed by digestion of P3 fraction from AD brain homogenates with increasing amounts of PK. Samples belonging to AP1 subgroup and the sAD1 case showed very high resistance to degradation, since increasing doses of PK (up to 100  $\mu$ g/ml) did not affect A $\beta$  aggregates. Conversely, a clear dose-dependent PK degradation of A $\beta$  assemblies was observed in samples from the AP2 subgroup and the two patients carrying APP mutations (Fig. 5a,b, S3).

A similar effect was found for the digestion of A $\beta$  dimers (Fig. 5a,c), as AP1 subgroup and the sAD1 case were quite stable over increasing PK concentrations, AP2 underwent a dose-dependent proteolysis, and the dimers from the APP-mutated cases were partially degraded by PK.

These data indicate that differences in the A $\beta$  composition of amyloid may affect the proteolytic activity of endogenous proteases on A $\beta$  aggregates, making the A $\beta$  assemblies derived from distinct molecular subgroups of AD more or less stable.

**Intracerebral injection of brain extracts from human subgroups in mice results in distinctive pattern of amyloid deposition.** Finally we assessed whether different molecular subgroups of AD have different abilities to propagate the pathological process *in vivo*, when injected in animal models<sup>30</sup>. We found that moApp<sup>0/0</sup>/APP23<sup>+/-</sup>, intra-cerebrally inoculated at six months of age with brain homogenates selected among the molecular subgroups previously identified, developed brain amyloidoses with distinctive disease profiles as to morphology, regional distribution of amyloid deposits, and preferential parenchymal or vascular A $\beta$  deposition (Figs 6 and 7), indicating that the phenotypic diversity of human pathology can be maintained upon transmission to mice, even if without a close replication of the features characterizing human donor brains.

Interestingly, the severity of neuropathological changes induced in mice by the brain extracts belonging to different AD subgroups was different suggesting that A $\beta$  seeds contained in human brain homogenates have physicochemical properties affecting their ability in propagating amyloidosis in animal models (Figs 6 and 7). Indeed, AP1 subgroup was more effective than AP2 subgroup in inducing and propagating the disease (Fig. 6). The brain extracts from the two APP-mutated patients (AP3 subgroup) showed relevant dissimilarities and were separately illustrated in Figs 6 and 7. Seeds from the sAD1 case were also particularly aggressive (Fig. 6).

Human brain extracts from AP1 induced an amyloidosis characterized by intense amyloid burden, with amyloid aggregates consisting of small sized and diffuse plaques, strongly associated with diffuse CAA and

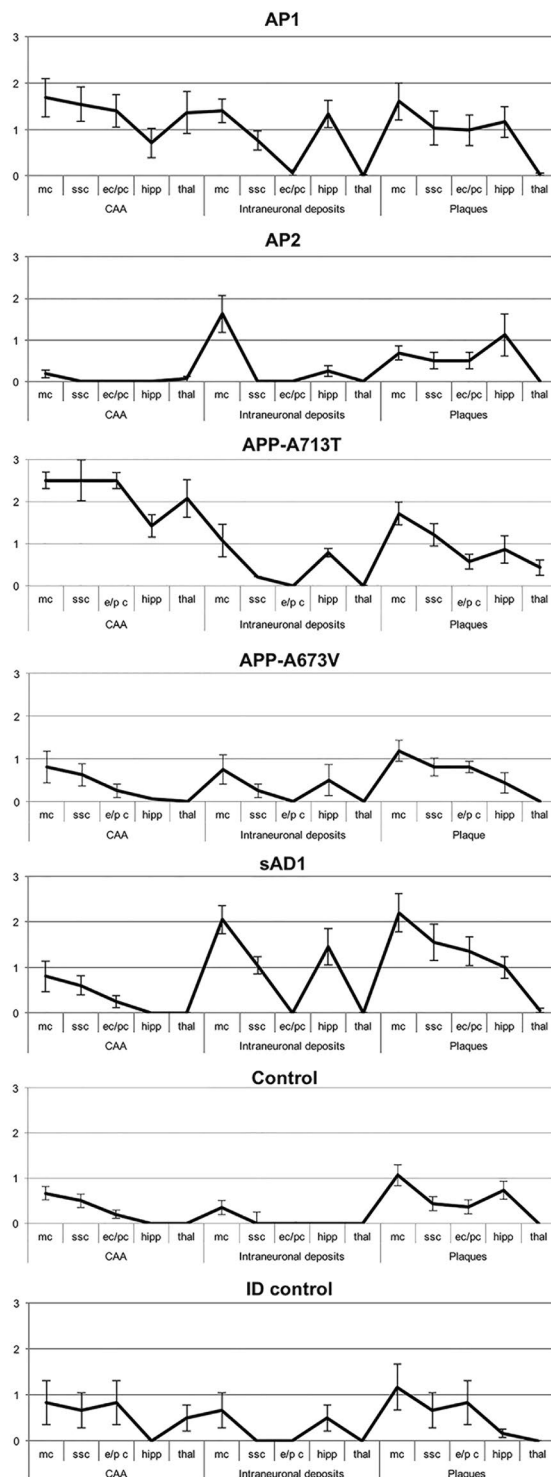


**Figure 6.** Lesion profiles in mice inoculated with human brain extracts from AD patients. CAA, intraneuronal A $\beta$  immunostaining and amyloid plaques were used to build up lesion profiles of the disease in mice. Control = untreated age-matched mice. mc = motor cortex; ssc = somato-sensory cortex; ec/pc = entorhinal cortex/piriform cortex; hipp = hippocampus; thal = thalamus. Immunohistochemical study was performed with 4G8 antibody. Quantification of 4G8 immunostaining was calculated by ‘plaque count’ method and expressed in each profile as a mean  $\pm$  SEM of the values obtained in animal groups (n = 8) injected with human brain extracts of each molecular profile: AP1-AP2 subgroups and APP<sub>A673V</sub> (fAD1), APP<sub>A713T</sub> (fAD2) and sAD1 case. Quantification by ‘plaque count’ was carried out using a scale ranging from 0 to 5 by light microscopy. The study was performed using “NIS-elements” software”.

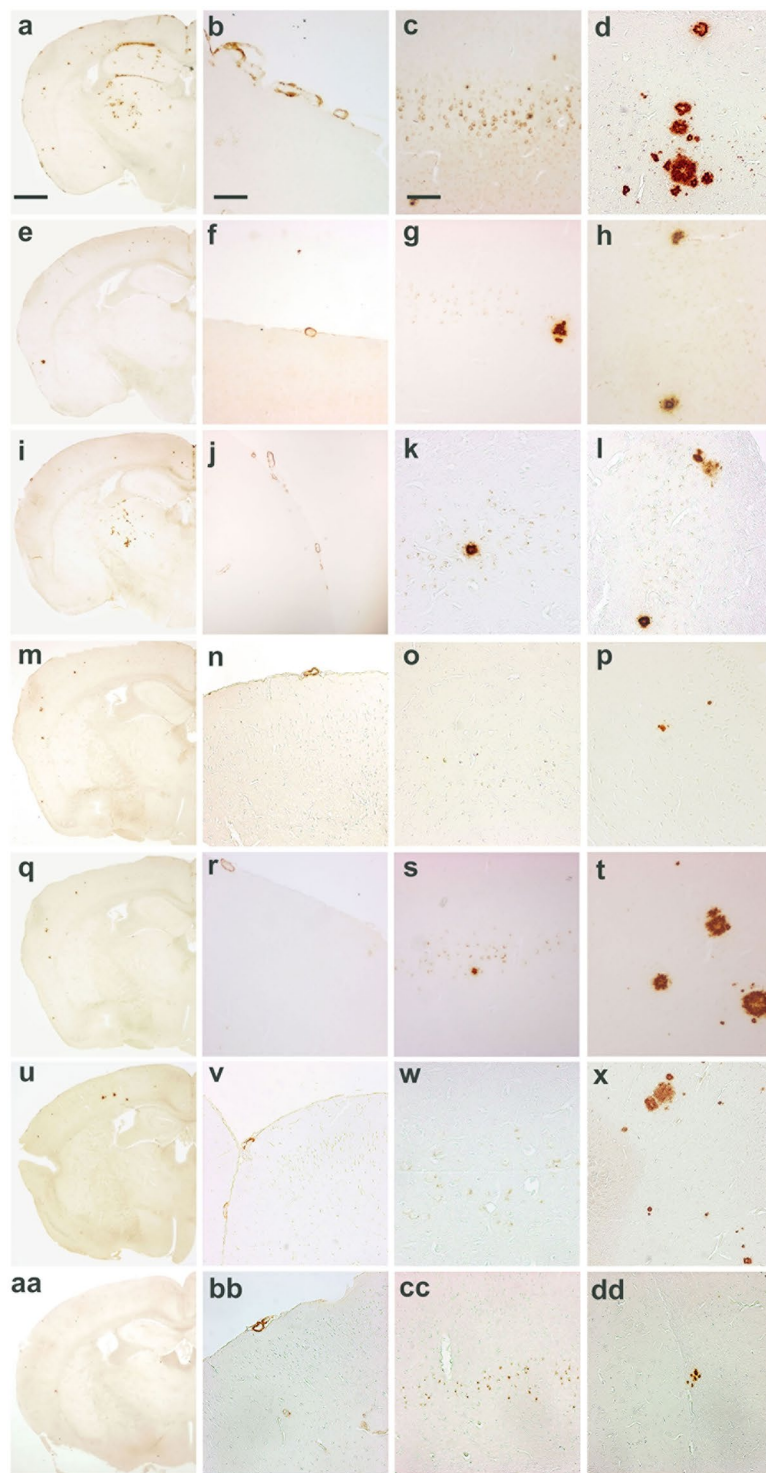


**Figure 7.** Amyloid burden in mice injected with human brain extracts from distinct molecular profiles of Alzheimer's disease. Mice inoculated with an Alzheimer brain homogenate from AP1 subgroup (**a–d**), AP2 subgroup (**e–h**), APP<sub>A713T</sub> (fAD2) (**i–l**), APP<sub>A673V</sub> (fAD1) (**m–p**), sAD1 case (**q–t**) and control groups, i.e. age-matched noninjected mice (**u–x**) and mice injected with A $\beta$ -immunodepleted brain extracts (**aa–dd**). (**a, e, i, m, q, u, aa**) Amyloid deposits, scale bar 0,5 mm. (**b, f, j, n, r, v, bb**) Congophilic amyloid angiopathy, 300  $\mu$ m. (**c, g, k, o, s, w, cc**) Intraneuronal A $\beta$  immunoreactivity, scale bar 120  $\mu$ m. (**d, h, l, p, t, x, dd**) Amyloid plaques, scale bar 120  $\mu$ m. Immunostaining with 4G8 antibody.

intraneuronal A $\beta$  immunoreactivity localized in hippocampus and neocortex (a-d panel in Fig. 7). In this group we observed abundant A $\beta$ -positive CAA with plaques within the thalamus, a peculiarity reported by Watts *et al.*<sup>31</sup> in APP23 mice inoculated with brain extracts derived from patients carrying the APP 'Artic' mutation.



Inoculation of AP2 samples resulted in a weaker and diffuse amyloid deposition, with faint CAA and intracellular immunostaining for A $\beta$ . The thalamus was not involved (e–h panels in Fig. 7).

Amyloidosis induced by APP<sub>A713T</sub> (fAD2) brain samples was characterized by low amyloid burden, high content of CAA, low amount of intraneuronal A $\beta$  immunostaining. Also in this group the lesion profile showed a thalamic deposition of A $\beta$  in vessel walls and, to lesser extent, in parenchymal deposits (i–l panels in Fig. 7). However, the pathologic changes in thalamus were less intense than in mice injected with AP1 brain extracts. APP<sub>A673V</sub> (fAD1) caused only a faint amyloidosis (m–p panels in Fig. 7).

Injection of brain extract from the sAD1 patient was associated with the highest amount of intraneuronal immunostaining for A $\beta$  especially present in hippocampus and motor cortex, diffuse parenchymal amyloid deposits showing large size, and less consistent CAA sparing thalamus (q–t panels in Fig. 7).

Intracerebral injection of human brain samples depleted of A $\beta$  seeds by immunodepletion did not modify the spontaneous amyloidogenesis of moApp<sup>0/0</sup>/APP23<sup>+/-</sup> mice (bottom panel in Fig. 6 and aa–dd panels in Fig. 7), confirming the view supported by previous reports<sup>26,32,33</sup> that A $\beta$  seeds are necessary to accelerate amyloidosis in the host. Inoculation of human extracts into nontransgenic littermate control mice was not associated with the development of amyloidosis. Injection of brain homogenate from a nondemented control did not modify the spontaneous amyloidogenesis of transgenic mice (data not shown). Finally, second passage inoculations of moApp<sup>0/0</sup>/APP23<sup>+/-</sup> mice were carried out. The resultant amyloidosis generated in animals retained the pathologic features induced by first passage injections in each experimental group, but showed a global attenuation of the severity of neuropathologic changes (data not shown), in line with previous studies demonstrating the resilience of A $\beta$  seeds<sup>34</sup>.

We also measured the levels of A $\beta$ 40 and A $\beta$ 42 in the insoluble fraction of brain homogenates from mice injected with human brain extracts. The results substantially confirmed the differences revealed by the neuropathological studies showing higher A $\beta$  levels in mice injected with AP1 subgroup, APP<sub>A713T</sub> and sAD1 patients. The AP2 subgroup and the APP<sub>A673V</sub> case showed lower amount of A $\beta$ . The immunodepleted controls had A $\beta$  levels similar to non-injected mice (Fig. S4).

## Discussion

Phenotypic heterogeneity of AD is a very complex phenomenon whose molecular basis is still largely unexplored. Recently, a correlation between A $\beta$  fibril structure and variations in AD phenotype has been demonstrated by solid-state nuclear magnetic resonance measurements on A $\beta$ 40 and A $\beta$ 42 fibrils prepared by seeded growth from AD brain extracts. These studies indicated that there is a qualitative difference between A $\beta$  aggregates in the brain tissue of patients with AD and that this difference may result in the generation of distinct disease phenotypes, in analogy to distinct prion strains that are associated with different phenotypes of prion diseases<sup>35</sup>.

Our study focused on one of the molecular aspects which might lead to the generation of differences in the structural properties of A $\beta$  assemblies that in turn may be involved in generation of distinct disease phenotypes. We found that: (i) amyloid- $\beta$  is generated starting from different mixtures of A $\beta$  peptides that participate in the amyloid biochemical composition; (ii) different subtypes of amyloid- $\beta$  might undergo distinct aggregation pathways, generating A $\beta$  assemblies that display different toxic properties, depending on the time-course of the lag and growth phases in their aggregation kinetics; (iii) amyloid subtypes also show variability in their seeding activity on monomeric A $\beta$ 1–42, which depends on the seed-substrate affinity during the polymerization process; (iv) aggregates from different amyloid- $\beta$  subtypes have diverging resistance to degradation by proteases, giving rise to assemblies that can be variably stable and toxic *in vivo*; (v) amyloid subtypes have differential ability toward anticipating or accelerating amyloidogenesis in animal models of AD and generate amyloidosis showing distinct features in mice injected with human brain extracts.

Moreover, it's conceivable that unknown environmental elements in the host brain tissue may be involved in modeling the pathologic changes of human brain-induced amyloidosis in mice, so explaining why the mouse pathology is not the simple replication of the human pathology.

The finding that genetic forms of the disease (i.e., those associated with APP mutations) have a molecular profile distinct from sporadic cases is not surprising, but our data support the view that molecular heterogeneity is a feature of sporadic forms too<sup>14,36–38</sup>.

Interestingly, amyloid profile enriched in A $\beta$ x-42 peptides (i.e., AP1) showed fast aggregation kinetics, strong seeding abilities, high resistance to proteolysis and aggressiveness in animal models. However, the high amount of the longest A $\beta$  isoform (i.e., A $\beta$ 1–42) in this subgroup cannot fully explain the aggressiveness of AP1 A $\beta$  seeds. Indeed, sAD1 case, which is characterized by a prevalence of A $\beta$ x-40 peptides, actually showed the most aggressive molecular phenotype. On the other hand, A $\beta$  seeds from patients carrying APP mutations (AP3 in our molecular grouping) displayed a heterogeneous behavior, one (APP<sub>A713T</sub>) being more aggressive, the other (APP<sub>A673V</sub>) showing only faint aggregation and seeding abilities, and inducing weak amyloid deposition in mice injected with its brain extracts. These last findings are in line with the results of several studies indicating that the heterologous interaction between wt and A673V-mutated A $\beta$  peptides results in inhibition of A $\beta$  polymerization<sup>39,40</sup>.

These results suggest that seeding and aggregation properties, resistance to proteolysis and aggressiveness of the neuropathological phenotype induced in animal models are caused by the differences in the A $\beta$  content that typify each AD subgroup.

Overall these data led to the recognition of 2 main distinct molecular profiles of the disease in the series of sporadic AD cases included in our study and supported a molecular clustering of AD based on the structural and functional properties of the ‘amyloids’ identified in each subgroup.

The overall data obtained by RT-QuIC assays supported the view that the differences in the aggregation profiles are not simply due to the quantities of A $\beta$ 40 or A $\beta$ 42 in the substrate source of brain tissue (i.e., soluble fraction of brain homogenates), but are reasonably influenced by the nature (i.e., biochemical content) of the initial seeds which trigger A $\beta$  polymerization as well as by the affinity between seed and substrate. Indeed, sAD1, which

contains much more A $\beta$ 40 than A $\beta$ 42 species, greatly promotes A $\beta$ 1–42 polymerization even more than the AP1 subgroup that is much more enriched in A $\beta$ 42 isoforms.

The data on sAD1 case further support our hypothesis that some differences in the *sporadic* AD subgroups may be related to intrinsic properties of the peptides involved into the aggregation kinetics. Based on this hypothesis, a certain mixture of A $\beta$  peptides may follow an aggregation pathway distinct from another mixture, leading to cerebral amyloidosis with distinctive characteristics. The peculiar features displayed by the sAD1 case also suggest that other variant AD subgroups may exist.

Intriguingly, two very recent papers suggested a structural variability of A $\beta$  aggregates in both sporadic and familial AD patients, supporting our hypothesis on the existence of distinct AD molecular subtypes<sup>41,42</sup>.

Phenotypic differences in AD stem from the interaction of a series of elements including genes that modulate the risk of developing the disease (such as *ApoE*) and less known environmental factors<sup>43,44</sup> which, together with predisposing components, may write the history of the disease as different clinical and pathological traits. In our study, we did not find a correlation between *ApoE* genotype and amyloid profile. Further studies on larger cohorts of patients and controls are needed to address this point.

Use of transmission studies for the identification and characterization of different forms of the disease is a yet poorly explored approach in the field of AD<sup>31</sup>. It has been successfully used for prion diseases to unveil the existence of different prion strains responsible for different prion-related pathologies<sup>45</sup>. Our study stems from previous evidence that amyloid deposition can be induced by injection of human brain extracts into animals which develop a cerebral amyloidosis involving also brain areas far from the injection site<sup>26,33,46</sup>. These data suggest that the typical brain abnormalities associated with AD can be induced by a prion-like mechanism based on the propagation of protein misfolding across brain tissue. Moreover, phenotypic variability is a salient feature of prion diseases where it is clearly sustained by the existence of distinct subtypes of prions<sup>47,48</sup>. These observations remind to the general concept of prion-like induction and spreading of pathogenic proteins that has been recently expanded to include aggregates of tau,  $\alpha$ -synuclein, huntingtin, superoxide dismutase-1, and TDP-43, which characterize several human neurodegenerative disorders such as frontotemporal lobar degeneration, Parkinson's/Lewy body disease, Huntington's disease and amyotrophic lateral sclerosis<sup>46,49,50</sup>. Noteworthy, all these diseases can present under different phenotypes, but the role of the disease-related misfolding proteins in the generation of their phenotypic variability has not yet been explained<sup>51,52</sup>.

Misfolding of PrP is the result of the intrinsic property of the prion protein to adopt different conformations, and generate different conformers of the protein, which can give rise to different subtypes of prionopathies<sup>53</sup>. Our data suggest the view that AD exists as distinct molecular phenotypes as a result of differences in the mixture of peptides participating in A $\beta$  assemblies.

Noteworthy, the variances in the amyloid composition offer a sort of bar code to identify different molecular AD subgroups.

We recently demonstrated that the preferential accumulation of some A $\beta$  fragments in amyloid was paralleled by a reduction of the very same fragments in the CSF of AD cases. This offers grounds to the detection of distinct AD subgroups by the analysis of A $\beta$  profile in CSF of AD patients<sup>54</sup>.

The comprehension of the molecular machinery responsible for the phenotypic diversity in AD is still at the beginning of its history, but it is becoming an urgent need, considering the emerging evidence that the different responsiveness to pharmacological treatments among AD cases could be due at least in part to the existence of distinct subgroups of the disease<sup>55,56</sup> diverging for their clinico-pathological, biochemical profiles, and pathogenic pathways too. The relevance of molecular heterogeneity of A $\beta$  assemblies in the generation of specific clinico-pathological AD phenotypes needs further studies in larger cohorts of patients. However, our study may help to understand the molecular bases of disease heterogeneity and design more appropriate therapies based on recognition of different target phenotypes.

## Materials and Methods

**Selection and neuropathological characterization of AD cases.** Informed consent was obtained from all individual participants included in the study. All procedures were in accordance with the 1964 Declaration of Helsinki and its later amendments and were approved by Ethical Committee of Carlo Besta Neurological Institute. Characterization of AD cases (n = 24) was primarily based on their neuropathological profiles and in consideration of burden, morphology and distribution of amyloid plaques, relative percentage of parenchymal and vascular deposits, immunoreactivity for a panel of antibodies to epitopes of different A $\beta$  domains<sup>7</sup> (see 'Materials and Methods' section in *Supplementary Information* for details). The *ApoE* genotype was determined in all cases. Genetically inherited AD cases were identified as fAD1 to fAD4. Sporadic cases were identified as sAD1 through sAD20. See Table S1 in *Supplementary Information* for details.

**Amyloid extraction. Complete protocol.** Amyloid was purified from frozen brain tissue of five AD cases following a method previously described for PrP amyloid<sup>57</sup> and applied to  $\beta$ -amyloid. In particular, 8 g of frontal cortex were serially homogenized in 9 volumes of buffer A (10 mM Tris-HCl, Sigma-Aldrich, St. Louis, MO pH 7.5, 150 mM NaCl, Sigma-Aldrich, St. Louis, MO, 1% Triton X-100, Amresco, Solon, OH, aded with Complete Protease Inhibitors cocktail, Roche, Mannheim, Germany), buffer B (10 mM Tris-HCl pH 7.5, 0.6 M KI, Sigma-Aldrich, St. Louis, MO, 0.5% Triton X-100, Complete Protease Inhibitors cocktail) and buffer C (10 mM Tris-HCl pH 7.5, 1.5 M KCl, Sigma-Aldrich, St. Louis, MO, 0.5% Triton X-100, Complete Protease Inhibitors cocktail). After each step, the homogenate was centrifuged at 10,000 xg for 40 minutes at 4 °C. The pellet was washed four times in buffer D (50 mM Tris-HCl, 150 mM NaCl, pH 7.5), centrifuged at 55,000 xg for 40 minutes at 4 °C, and digested with Collagenase Type1 at 37 °C for 18 hours. After centrifugation at 70,000 xg for 1 hour at 4 °C, the pellet was washed three times in 50 mM Tris-HCl pH 7.5, loaded on a discontinuous sucrose gradient (1.0, 1.2, 1.4, 1.7, 2.0 M sucrose, Sigma-Aldrich, St. Louis, MO, in 10 mM Tris-HCl pH 7.5) and centrifuged at

130,000  $\times g$  for 2 hours at 20 °C. Each interface was collected, washed three times in buffer D and centrifuged at 55,000  $\times g$  for 30 minutes at 4 °C. Amyloid was extracted with 80% formic acid, Sigma-Aldrich, St. Louis, MO, dried and re-suspended in H<sub>2</sub>O for further analysis.

**Simplified protocol.** A simplified amyloid extraction protocol was applied to the same five AD cases. Briefly, three hundred mg of frontal cortex were homogenized in 9 volumes of 10 mM Tris-HCl, pH 7.5, 0.5% Triton X-100 added with Complete Protease Inhibitors cocktail using a manual Dounce homogenizer, sonicated for 2 minutes using a Ultrasonic homogenizer Sonopuls-series HD2070 and centrifuged at 3,000  $\times g$  for 5 minutes at 4 °C. The supernatant was loaded on a discontinuous sucrose gradient (1.0, 1.4, 1.8 M sucrose in 10 mM Tris-HCl pH 7.5) and centrifuged at 130,000  $\times g$  for 2 hours at 20 °C. Each interface was collected, washed three times in 50 mM Tris-HCl, 150 mM NaCl, pH 7.5 and centrifuged at 55,000  $\times g$  for 30 minutes at 4 °C. The pellet was treated with 80% formic acid, dried and re-suspended in H<sub>2</sub>O for further analysis.

No substantial differences were observed between amyloid samples obtained by full and simplified sucrose-gradient fractionation protocols (data not shown). So, we used the simplified procedure to extract amyloid from all other AD cases and controls.

**Immunoproteomic analyses.** The immunoproteomic assay for A $\beta$  isoforms detection was performed as previously reported<sup>58</sup>, with minor modifications. Briefly, 3  $\mu$ l of a 0.125 mg/ml monoclonal antibody solution (6E10 and 4G8, Covance, Dedham, MA) was incubated for 3 h at room temperature in a humidity chamber to allow covalent binding to the PS20 ProteinChip Array (Bio-RAD Laboratories Inc., Hercules, CA). Unreacted sites were blocked for 1 h at room temperature with 0.4 M Tris-HCl, pH 8.0, in a humidity chamber. Each spot was washed three times with PBS containing 0.5% (v/v) Triton X-100 then twice with PBS alone. Spots were coated with 5  $\mu$ l of sample and incubated at 4 °C overnight in a humidity chamber before being washed three times with PBS containing 0.1% (v/v) Triton X-100, twice with PBS alone and finally with deionized water. 1.2  $\mu$ l of  $\alpha$ -cyano-4-hydroxy cinnamic acid (Bio-RAD Laboratories, Inc., Hercules, CA) was added to each spot and mass identification was performed using the ProteinChip SELDI System, Enterprise Edition (Bio-RAD Laboratories, Inc., Hercules, CA). The different amyloid profiles characterizing each AD subgroup were identified taking into account the relative percentage of the different A $\beta$  isoforms detected by SELDI-TOF MS.

**Brain homogenates.** Brain homogenates were prepared as previously described<sup>59</sup>. Briefly, 200 mg of frontal cortex were homogenized in 5 volumes of 20 mM Tris-HCl, pH 7.5, 140 mM NaCl, added with Complete Protease Inhibitors cocktail and Phosphatase Inhibitors Cocktail 2 (Sigma) using a manual Dounce homogenizer and ultracentrifuged at 100,000  $\times g$  for 1 hour at 4 °C. The supernatant was collected, aliquoted and stored at -80 °C as the S1 fraction. The pellet was re-homogenized in 1% Chaps, 1% Deoxycholate, 0.2% SDS, 140 mM NaCl, 10 mM Tris-HCl, pH 7.5, added with Protease and Phosphatase Inhibitors and ultracentrifuged at 30,000  $\times g$  for 30 minutes at 4 °C. The supernatant was aliquoted and stored at -80 °C as the S2 fraction; the pellet was homogenized in 2% SDS, 20 mM Tris-HCl, pH 7.5, 140 mM NaCl and ultracentrifuged at 30,000  $\times g$  for 30 minutes at 4 °C. The supernatant was saved as the S3 fraction and stored at -80 °C; the pellet was extracted in 4% SDS, 8 M Urea (P3 fraction). The total proteins amount was measured in each fraction by BCA Protein Assay kit (Pierce). Immunodepletion was carried out by using Protein G Mag Sepharose beads (GE Healthcare) and a mixture of 4G8 and 6E10 antibodies.

**Thioflavin T aggregation assay.** 5 microliters of brain homogenates' soluble fractions (S1) were diluted in 100 mM Tris-HCl pH 7.5, 5  $\mu$ M ThT, and transferred in triplicate into wells of a black, clear bottom, 96-well microplate (Nunc). The plate was incubated at 25 °C into a BMG Fluostar Optima Microplate Reader (BMG Labtech). Every 59 minutes the plate was shaken for 1 minute and the fluorescence was measured. For the comparison of aggregation kinetics among A $\beta$  extracted from different AD brains, we considered the slope of the curve described by fluorescence values at different time points.

A preliminary step in the ThT assays was used to test the effects of the initial quantity of soluble A $\beta$  in AD brain extracts on the shape of aggregation curves. To this end, 5 or 10 microliters of brain homogenates' soluble fractions (S1) of some human brain samples were analyzed by ThT assay and showed overlapping profiles.

**Real-Time Quaking-Induced Conversion (RT-QuIC) assay.** For these assays, a previously described protocol<sup>60</sup> - not yet fully validated - was used. It was slightly modified in order to comply with the analysis of brain samples.

5 microliters of brain homogenates' S1 fractions were used as *seeds* and diluted in 100 mM Tris-HCl pH 7.5, 5  $\mu$ M ThT, 4  $\mu$ M synthetic A $\beta$ 1-42<sub>WT</sub> or A $\beta$ 1-42<sub>A2V</sub>. The reactions were transferred in quadruplicate into wells of a black, clear bottom, 96-well microplate (Nunc). The plate was incubated at 37 °C into a BMG Fluostar Optima Microplate Reader (BMG Labtech), and shaken every other minute. Fluorescence was measured every 15 minutes. The same protocol was used to test the seeding ability of brain extracts on A $\beta$ 1-40<sub>WT</sub>, except for A $\beta$ 1-40 concentration (10  $\mu$ M) and incubation temperature (30 °).

**Sensitivity to PK digestion.** For proteinase K (PK) digestion, 5 micrograms (or 1 microgram for patients carrying A673V and A713T APP mutations) of total proteins from P3 fractions were digested with increasing levels (between 0 and 100  $\mu$ g/ml) of PK for 1 hour at 37 °C. PK digestion was blocked by adding Bolt LDS Sample Buffer (Invitrogen) and Bolt Sample Reducing Agent (Invitrogen) and incubating 10 minutes at 70 °C; the samples were analyzed by Western blot.

**Western blot.** Samples were loaded on Bolt 4–12% Bis-Tris polyacrylamide gels (Invitrogen), transferred to PVDF and immunoblotted with 4G8 (Signet) diluted 1:1000. The membranes were then sequentially incubated with biotin-goat anti-mouse (Invitrogen) and Streptavidin-horseradish peroxidase conjugate (GE Healthcare) and revealed using ECL Prime (GE Healthcare). The signal intensity was quantified by densitometry using the software Quantity One (BioRad).

**Transmission studies.** The experimental procedures using mice were carried out in accordance with the veterinary office regulations established by both the Council of Europe Convention ETS123 (European Convention for the Protection of Vertebrate Animals used for Experimental and Other Scientific Purposes; Strasbourg, 18.03.1986) and the European directive 2010/63 transposed in Italian D.L.vo 26/14. The study was approved by Italian Ministry of Health (approval number 1219/2015-PR).

Whole brain homogenates from AD cases belonging to the different molecular subtypes recognized by biochemical studies (AP1-AP3 and the sAD1 case) and two controls (one age-matched nondemented subject and one AD brain homogenate deprived from A $\beta$  by immunodepletion with anti-A $\beta$  antibodies) were prepared as follows. Samples of frontal cortex were homogenized in 9 volumes of sterile 1 $\times$  PBS using a manual Dounce homogenizer, sonicated for 15 seconds using an Ultrasonic homogenizer Sonopuls-series HD2070 and centrifuged at 3,000 xg for 5 minutes at 4 °C. The supernatants were collected, aliquoted and stored at –80 °C until inoculation in APP23 mice (carrying the double Swedish human APP mutation), knock-out for endogenous App (moApp<sup>0/0</sup>/APP23<sup>+/-</sup>), chosen to avoid the interference of murine App in the propagation of the disease. See *Supplementary Information* for details.

**Statistical analysis.** Student t-test was used to compare amyloid burden in immunohistochemical studies on human brains and on brains from mice inoculated with human cerebral homogenates. The densitometric data obtained from the quantification of Western Blot for the study of PK resistance were compared by two-ways ANOVA. Kruskal-Wallis followed by Dunn's multiple comparison test was used to compare A $\beta$ 40 and A $\beta$ 42 levels measured by ELISA in the insoluble fractions of injected mice. Two tailed P value less than 0.05 was considered statistically significant. All calculations were performed using GraphPad Prism 5.

**Data availability statement.** The datasets generated during and/or analyzed during the current study are available from the corresponding author on reasonable request.

**Ethical approval.** All procedures performed in studies involving human participants were in accordance with the ethical standards of the institutional and/or national research committee and with the 1964 Helsinki declaration and its later amendments. All applicable international, national, and/or institutional guidelines for the care and use of animals were followed.

## References

1. Watson, D. *et al.* Physicochemical characteristics of soluble oligomeric Abeta and their pathologic role in Alzheimer's disease. *Neurol Res* **27**, 869–881, <https://doi.org/10.1179/016164105X49436> (2005).
2. Hardy, J. A. & Higgins, G. A. Alzheimer's disease: the amyloid cascade hypothesis. *Science* **256**, 184–185 (1992).
3. Haass, C. & Selkoe, D. J. Soluble protein oligomers in neurodegeneration: lessons from the Alzheimer's amyloid beta-peptide. *Nat Rev Mol Cell Biol* **8**, 101–112, <https://doi.org/10.1038/nrm2101> (2007).
4. De Strooper, B. Proteases and proteolysis in Alzheimer disease: a multifactorial view on the disease process. *Physiol Rev* **90**, 465–494, <https://doi.org/10.1152/physrev.00023.2009> (2010).
5. Portelius, E. *et al.* Mass spectrometric characterization of brain amyloid beta isoform signatures in familial and sporadic Alzheimer's disease. *Acta Neuropathol* **120**, 185–193, <https://doi.org/10.1007/s00401-010-0690-1> (2010).
6. Duyckaerts, C., Delatour, B. & Potier, M. C. Classification and basic pathology of Alzheimer disease. *Acta Neuropathol* **118**, 5–36, <https://doi.org/10.1007/s00401-009-0532-1> (2009).
7. Hyman, B. T. *et al.* National Institute on Aging-Alzheimer's Association guidelines for the neuropathologic assessment of Alzheimer's disease. *Alzheimers Dement* **8**, 1–13, <https://doi.org/10.1016/j.jalz.2011.10.007> (2012).
8. Di Fede, G., Giaccone, G. & Tagliavini, F. Hereditary and sporadic beta-amyloidosis. *Front Biosci (Landmark Ed)* **18**, 1202–1226 (2013).
9. De Felice, F. G. *et al.* Alzheimer's disease-type neuronal tau hyperphosphorylation induced by A beta oligomers. *Neurobiol Aging* **29**, 1334–1347, <https://doi.org/10.1016/j.neurobiolaging.2007.02.029> (2008).
10. Guglielmotto, M. *et al.* A $\beta$ 1–42 monomers or oligomers have different effects on autophagy and apoptosis. *Autophagy* **10**, 1827–1843, <https://doi.org/10.4161/auto.30001> (2014).
11. Jin, M. *et al.* Soluble amyloid beta-protein dimers isolated from Alzheimer cortex directly induce Tau hyperphosphorylation and neuritic degeneration. *Proc Natl Acad Sci USA* **108**, 5819–5824, <https://doi.org/10.1073/pnas.1017033108> (2011).
12. Hellström-Lindahl, E., Viitanen, M. & Marutle, A. Comparison of Abeta levels in the brain of familial and sporadic Alzheimer's disease. *Neurochem Int* **55**, 243–252, <https://doi.org/10.1016/j.neuint.2009.03.007> (2009).
13. Bitan, G. *et al.* Amyloid beta-protein (Abeta) assembly: Abeta 40 and Abeta 42 oligomerize through distinct pathways. *Proc Natl Acad Sci USA* **100**, 330–335, <https://doi.org/10.1073/pnas.222681699> (2003).
14. De Kimpe, L. & Scheper, W. From alpha to omega with Abeta: targeting the multiple molecular appearances of the pathogenic peptide in Alzheimer's disease. *Curr Med Chem* **17**, 198–212 (2010).
15. Larner, A. J. "Frontal variant Alzheimer's disease": a reappraisal. *Clin Neurol Neurosurg* **108**, 705–708, <https://doi.org/10.1016/j.clineuro.2005.07.001> (2006).
16. Nelson, P. T. *et al.* Correlation of Alzheimer disease neuropathologic changes with cognitive status: a review of the literature. *J Neuropathol Exp Neurol* **71**, 362–381, <https://doi.org/10.1097/NEN.0b013e31825018f7> (2012).
17. Levine, H. & Walker, L. C. Molecular polymorphism of Abeta in Alzheimer's disease. *Neurobiol Aging* **31**, 542–548, <https://doi.org/10.1016/j.neurobiolaging.2008.05.026> (2010).
18. Piccini, A. *et al.* Beta-amyloid is different in normal aging and in Alzheimer disease. *J Biol Chem* **280**, 34186–34192, <https://doi.org/10.1074/jbc.M501694200> (2005).
19. Maarouf, C. L. *et al.* Histopathological and molecular heterogeneity among individuals with dementia associated with Presenilin mutations. *Mol Neurodegener* **3**, 20, <https://doi.org/10.1186/1750-1326-3-20> (2008).



20. Nilsson, K. P. *et al.* Imaging distinct conformational states of amyloid-beta fibrils in Alzheimer's disease using novel luminescent probes. *ACS Chem Biol* **2**, 553–560, <https://doi.org/10.1021/cb700116u> (2007).
21. Miners, J. S., Jones, R. & Love, S. Differential changes in A $\beta$ 42 and A $\beta$ 40 with age. *J Alzheimers Dis* **40**, 727–735, <https://doi.org/10.3233/JAD-132339> (2014).
22. Vidal, R. & Ghetti, B. Characterization of amyloid deposits in neurodegenerative diseases. *Methods Mol Biol* **793**, 241–258, [https://doi.org/10.1007/978-1-61779-328-8\\_16](https://doi.org/10.1007/978-1-61779-328-8_16) (2011).
23. Paravastu, A. K., Qahwash, I., Leapman, R. D., Meredith, S. C. & Tycko, R. Seeded growth of beta-amyloid fibrils from Alzheimer's brain-derived fibrils produces a distinct fibril structure. *Proc Natl Acad Sci USA* **106**, 7443–7448, <https://doi.org/10.1073/pnas.0812033106> (2009).
24. Lu, J. X. *et al.* Molecular structure of  $\beta$ -amyloid fibrils in Alzheimer's disease brain tissue. *Cell* **154**, 1257–1268, <https://doi.org/10.1016/j.cell.2013.08.035> (2013).
25. Jucker, M. & Walker, L. C. Self-propagation of pathogenic protein aggregates in neurodegenerative diseases. *Nature* **501**, 45–51, <https://doi.org/10.1038/nature12481> (2013).
26. Meyer-Luehmann, M. *et al.* Exogenous induction of cerebral beta-amyloidogenesis is governed by agent and host. *Science* **313**, 1781–1784, <https://doi.org/10.1126/science.1131864> (2006).
27. Bolmont, T. *et al.* Induction of tau pathology by intracerebral infusion of amyloid- $\beta$ -containing brain extract and by amyloid- $\beta$  deposition in APP x Tau transgenic mice. *Am J Pathol* **171**, 2012–2020, <https://doi.org/10.2353/ajpath.2007.070403> (2007).
28. Heilbronner, G. *et al.* Seeded strain-like transmission of  $\beta$ -amyloid morphotypes in APP transgenic mice. *EMBO Rep* **14**, 1017–1022, <https://doi.org/10.1038/embor.2013.137> (2013).
29. Giaccone, G. *et al.* Neuropathology of the recessive A673V APP mutation: Alzheimer disease with distinctive features. *Acta Neuropathol* **120**, 803–812, <https://doi.org/10.1007/s00401-010-0747-1> (2010).
30. Stöhr, J. *et al.* Distinct synthetic A $\beta$  prion strains producing different amyloid deposits in bigenic mice. *Proc Natl Acad Sci USA* **111**, 10329–10334, <https://doi.org/10.1073/pnas.1408968111> (2014).
31. Watts, J. C. *et al.* Serial propagation of distinct strains of A $\beta$  prions from Alzheimer's disease patients. *Proc Natl Acad Sci USA* **111**, 10323–10328, <https://doi.org/10.1073/pnas.1408900111> (2014).
32. Duran-Aniotz, C. *et al.* Aggregate-depleted brain fails to induce A $\beta$  deposition in a mouse model of Alzheimer's disease. *PLoS One* **9**, e89014, <https://doi.org/10.1371/journal.pone.0089014> (2014).
33. Langer, F. *et al.* Soluble A $\beta$  seeds are potent inducers of cerebral  $\beta$ -amyloid deposition. *J Neurosci* **31**, 14488–14495, <https://doi.org/10.1523/JNEUROSCI.3088-11.2011> (2011).
34. Ye, L. *et al.* Persistence of A $\beta$  seeds in APP null mouse brain. *Nat Neurosci* **18**, 1559–1561, <https://doi.org/10.1038/nn.4117> (2015).
35. Qiang, W., Yau, W. M., Lu, J. X., Collinge, J. & Tycko, R. Structural variation in amyloid-beta fibrils from Alzheimer's disease clinical subtypes. *Nature* **541**, 217–221, <https://doi.org/10.1038/nature20814> (2017).
36. Janocko, N. J. *et al.* Neuropathologically defined subtypes of Alzheimer's disease differ significantly from neurofibrillary tangle-predominant dementia. *Acta Neuropathol* **124**, 681–692, <https://doi.org/10.1007/s00401-012-1044-y> (2012).
37. Warren, J. D., Fletcher, P. D. & Golden, H. L. The paradox of syndromic diversity in Alzheimer disease. *Nat Rev Neurol* **8**, 451–464, <https://doi.org/10.1038/nrneurol.2012.135> (2012).
38. Rossor, M. N., Fox, N. C., Freeborough, P. A. & Harvey, R. J. Clinical features of sporadic and familial Alzheimer's disease. *Neurodegeneration* **5**, 393–397 (1996).
39. Di Fede, G. *et al.* A recessive mutation in the APP gene with dominant-negative effect on amyloidogenesis. *Science* **323**, 1473–1477, <https://doi.org/10.1126/science.1168979> (2009).
40. Di Fede, G. *et al.* Good gene, bad gene: new APP variant may be both. *Prog Neurobiol* **99**, 281–292, <https://doi.org/10.1016/j.pneurobio.2012.06.004> (2012).
41. Rasmussen, J. *et al.* Amyloid polymorphisms constitute distinct clouds of conformational variants in different etiological subtypes of Alzheimer's disease. *Proc Natl Acad Sci USA* **114**, 13018–13023, <https://doi.org/10.1073/pnas.1713215114> (2017).
42. Condello, C. *et al.* Structural heterogeneity and intersubject variability of Abeta in familial and sporadic Alzheimer's disease. *Proc Natl Acad Sci USA*, <https://doi.org/10.1073/pnas.1714966115> (2018).
43. Lahiri, D. K., Sambamurti, K. & Bennett, D. A. Apolipoprotein gene and its interaction with the environmentally driven risk factors: molecular, genetic and epidemiological studies of Alzheimer's disease. *Neurobiol Aging* **25**, 651–660, <https://doi.org/10.1016/j.neurobiolaging.2003.12.024> (2004).
44. Mastroeni, D. *et al.* Epigenetic mechanisms in Alzheimer's disease. *Neurobiol Aging* **32**, 1161–1180, <https://doi.org/10.1016/j.neurobiolaging.2010.08.017> (2011).
45. Watts, J. C. & Prusiner, S. B. Mouse models for studying the formation and propagation of prions. *J Biol Chem* **289**, 19841–19849, <https://doi.org/10.1074/jbc.R114.550707> (2014).
46. Jucker, M. & Christen, Y. *Proteopathic Seeds and Neurodegenerative Diseases*. (Heidelberg: Springer, 2013).
47. Prusiner, S. B., Scott, M. R., DeArmond, S. J. & Cohen, F. E. Prion protein biology. *Cell* **93**, 337–348 (1998).
48. Parchi, P., Strammiello, R., Giese, A. & Kretzschmar, H. Phenotypic variability of sporadic human prion disease and its molecular basis: past, present, and future. *Acta Neuropathol* **121**, 91–112, <https://doi.org/10.1007/s00401-010-0779-6> (2011).
49. Goedert, M. NEURODEGENERATION. Alzheimer's and Parkinson's diseases: The prion concept in relation to assembled A $\beta$ , tau, and  $\alpha$ -synuclein. *Science* **349**, 1255555, <https://doi.org/10.1126/science.1255555> (2015).
50. Clavaguera, F., Hench, J., Goedert, M. & Tolnay, M. Invited review: Prion-like transmission and spreading of tau pathology. *Neuropathol Appl Neurobiol* **41**, 47–58, <https://doi.org/10.1111/nan.12197> (2015).
51. Cohen, M., Appleby, B. & Safar, J. G. Distinct Prion-Like Strains of Amyloid Beta Implicated in Phenotypic Diversity of Alzheimer Disease. *Prion*, 0, <https://doi.org/10.1080/19336896.2015.1123371> (2016).
52. Cohen, M. L. *et al.* Rapidly progressive Alzheimer's disease features distinct structures of amyloid- $\beta$ . *Brain* **138**, 1009–1022, <https://doi.org/10.1093/brain/awv006> (2015).
53. Puoti, G. *et al.* Sporadic human prion diseases: molecular insights and diagnosis. *Lancet Neurol* **11**, 618–628, [https://doi.org/10.1016/S1474-4422\(12\)70063-7](https://doi.org/10.1016/S1474-4422(12)70063-7) (2012).
54. Catania, M. *et al.* Mirror Image of the Amyloid- $\beta$  Species in Cerebrospinal Fluid and Cerebral Amyloid in Alzheimer's Disease. *J Alzheimers Dis* **47**, 877–881, <https://doi.org/10.3233/JAD-150179> (2015).
55. Poirier, J. *et al.* Apolipoprotein E4 allele as a predictor of cholinergic deficits and treatment outcome in Alzheimer disease. *Proc Natl Acad Sci USA* **92**, 12260–12264 (1995).
56. Vega, G. L. *et al.* The effects of gender and CYP46 and apo E polymorphism on 24S-hydroxycholesterol levels in Alzheimer's patients treated with statins. *Curr Alzheimer Res* **1**, 71–77 (2004).
57. Tagliavini, F. *et al.* Amyloid protein of Gerstmann-Sträussler-Scheinker disease (Indiana kindred) is an 11 kd fragment of prion protein with an N-terminal glycine at codon 58. *EMBO J* **10**, 513–519 (1991).
58. Albertini, V. *et al.* Optimization protocol for amyloid- $\beta$  peptides detection in human cerebrospinal fluid using SELDI TOF MS. *Proteomics Clin Appl* **4**, 352–357 (2010).
59. Jimenez, S. *et al.* Disruption of amyloid plaques integrity affects the soluble oligomers content from Alzheimer disease brains. *PLoS One* **9**, e114041, <https://doi.org/10.1371/journal.pone.0114041> (2014).
60. Salvadores, N., Shah Nawaz, M., Scarpini, E., Tagliavini, F. & Soto, C. Detection of misfolded Abeta oligomers for sensitive biochemical diagnosis of Alzheimer's disease. *Cell Rep* **7**, 261–268, <https://doi.org/10.1016/j.celrep.2014.02.031> (2014).

## Acknowledgements

This study was supported by the Italian Ministry of Health NET-2011-02346784 (RF-175 2015–2018) (to F.T.) and RC (Current Research) to M.C., R.G., G.D.F., G.G. and L.B.), the REFRAME JPND grant from the EC Joint Programme on Neurodegenerative Diseases (to G.D.F.). B.G. was supported by U.S. Public Health Service (USPHS) P30 AG10133.

## Author Contributions

M.C. carried out most biochemical experiments. M.C., F.M., L.C. and E.B. carried out experiments on aggregation kinetics and seeding effects. G.G., E.M. and A.K. performed neuropathological studies. B.G. contributed to build the basic concept and to prepare the manuscript. I.C., M.C., S.S. and F.M. conducted injection of mice with A.D. brain extracts. R.G., L.B., A.P. and E.T. performed studies by SELDI-TOF MS. G.D.F. and F.T. designed and supervised the scientific work, and wrote the manuscript. All authors have read and approved the final version of this manuscript.

## Additional Information

**Supplementary information** accompanies this paper at <https://doi.org/10.1038/s41598-018-21641-1>.

**Competing Interests:** The authors declare no competing interests.

**Publisher's note:** Springer Nature remains neutral with regard to jurisdictional claims in published maps and institutional affiliations.



**Open Access** This article is licensed under a Creative Commons Attribution 4.0 International License, which permits use, sharing, adaptation, distribution and reproduction in any medium or format, as long as you give appropriate credit to the original author(s) and the source, provide a link to the Creative Commons license, and indicate if changes were made. The images or other third party material in this article are included in the article's Creative Commons license, unless indicated otherwise in a credit line to the material. If material is not included in the article's Creative Commons license and your intended use is not permitted by statutory regulation or exceeds the permitted use, you will need to obtain permission directly from the copyright holder. To view a copy of this license, visit <http://creativecommons.org/licenses/by/4.0/>.

© The Author(s) 2018